IJMMM International Journal of Minerals, Metallurgy and Materials 矿物冶金与材料学报（英文版）

Cross-upgrading of biomass hydrothermal carbonization and pyrolysis for high quality blast furnace injection fuel production: Physicochemical characteristics and gasification kinetics analysis

Han Dang, Runsheng Xu, Jianliang Zhang, Mingyong Wang, and Jinhua Li

Cite this article as:
Han Dang, Runsheng Xu, Jianliang Zhang, Mingyong Wang, and Jinhua Li, Cross-upgrading of biomass hydrothermal carbonization and pyrolysis for high quality blast furnace injection fuel production: Physicochemical characteristics and gasification kinetics analysis, *Int. J. Miner. Metall. Mater.*, 31(2024), No. 2, pp. 268-281. https://doi.org/10.1007/s12613-023-2728-0

View the article online at SpringerLink or IJMMM Webpage.

INTERNATIONAL JOURNAL OF
Minerals, Metallurgy and Materials

Volume 31, Number 2, February 2024
Page 268

Research Article https://doi.org/10.1007/s12613-023-2728-0

Cross-upgrading of biomass hydrothermal carbonization and pyrolysis for high quality blast furnace injection fuel production: Physicochemical characteristics and gasification kinetics analysis

Han Dang[1)], *Runsheng Xu*[1),✉], *Jianliang Zhang*[1,2)], *Mingyong Wang*[1)], *and Jinhua Li*[1),✉]

1) State Key Laboratory of Advanced Metallurgy, University of Science and Technology Beijing, Beijing 100083, China
2) School of Chemical Engineering, The University of Queensland, Queensland 4072, Australia
(Received: 4 May 2023; revised: 25 July 2023; accepted: 16 August 2023)

Abstract: The paper proposes a biomass cross-upgrading process that combines hydrothermal carbonization and pyrolysis to produce high-quality blast furnace injection fuel. The results showed that after upgrading, the volatile content of biochar ranged from 16.19% to 45.35%, and the alkali metal content, ash content, and specific surface area were significantly reduced. The optimal route for biochar production is hydrothermal carbonization–pyrolysis (P-HC), resulting in biochar with a higher calorific value, C=C structure, and increased graphitization degree. The apparent activation energy (E) of the sample ranges from 199.1 to 324.8 kJ/mol, with P-HC having an E of 277.8 kJ/mol, lower than that of raw biomass, primary biochar, and anthracite. This makes P-HC more suitable for blast furnace injection fuel. Additionally, the paper proposes a path for P-HC injection in blast furnaces and calculates potential environmental benefits. P-HC offers the highest potential for carbon emission reduction, capable of reducing emissions by 96.04 kg/t when replacing 40wt% coal injection.

Keywords: blast furnace injection; biomass; cross-upgrading; hydrothermal carbonization; pyrolysis; physicochemical properties; gasification properties

1. Introduction

Steel industry is a high energy consumption and high pollution industry, but it also has the greatest potential for energy conservation and emission reduction. However, in the foreseeable future, it is difficult to change the present situation of blast furnace–converter as the main steel production process [1–2]. At the same time, the excessive consumption of coal makes the energy consumption and pollutant emission of the ironmaking process occupy more than 70% of the whole production process [3–4]. As the Chinese government's goal of reaching the "carbon peak" and "carbon neutrality" is approaching, it is urgent to reduce pollution and carbon in the steel industry, develop low-carbon economy, and change the industrial energy structure [5].

As a carbon-neutral material, the global annual straw production is close to 4 billion tons, of which China accounts for about 25%. Chinese current biomass reserves are equivalent to 1 billion tons of standard coal [6–9]. If the biomass can be used as fuel in blast furnace, it can not only alleviate the consumption of coal resources, but also reduce carbon emissions [10]. However, some problems of biomass itself limit its large-scale application. Zhang [11] pointed out that biomass has good combustibility for direct-combustion power generation. However, the high content of inorganic impurities such as K and Cl will cause problems such as slagging in the boiler, ash deposition on the heated surface, chlorine corrosion on the low-temperature heating surface, and high-temperature corrosion of the superheater pipe during the direct combustion of biomass. Wang [12] conducted basic research on blast furnace injection of agricultural and forestry wastes, and the results show that the initial combustion temperature of straw powder is low and the combustion speed is fast. However, since the alkali oxides and salts in the straw ash can react with SiO_2 to form a low-temperature eutectic, the straw ash has a low melting point and is prone to tuyere coking, which is not suitable for independent injection. In addition, the energy density of biomass is low, the grindability is poor, and the alkali metal content is high, so it cannot be directly used as fuel in blast furnace injection [13]. Therefore, it is necessary to pretreat the biomass to increase the energy density and reduce alkali content.

Among the many biomass upgrading technologies, thermochemical conversion technology is the most feasible. Pyrolysis is the most common and mature thermochemical conversion technology for biomass upgrading. In terms of the application of biomass pyrolytic char as fuel in thermal power plants and ironmaking plants, the research results of

✉ Corresponding authors: Runsheng Xu E-mail: xu_runsheng@163.com; Jinhua Li E-mail: 1304503396@qq.com

many studies have shown that although pyrolysis can effectively improve the energy density of biomass, alkali accumulation exists in the pyrolysis process of biomass. Therefore, the ash content of the biomass pyrolytic char, mainly oxide of alkali, is much higher than that of the raw biomass samples [14]. High temperature corrosion of boiler and coking of BF tuyere caused by alkali can't be avoided by using biomass pyrolytic char in power plant and ironmaking plants. In recent years, hydrothermal carbonization (HTC) has attracted the attention of many researchers as an emerging technology for the preparation of biochar [15–16]. Hydrochar prepared by HTC has the characteristics of low alkali and ash content, which is exactly what pyrolysis doesn't have. However, the research results of some studies have shown that the volatile content of hydrochar is much higher than that of bituminous coal with strong explosive, and the specific surface area is also greater than coal, and the larger specific surface area increases the contact area between hydrochar and air, which makes the combustion reaction easier [17]. When the hydrochar is directly used in blast furnace injection, the ignition point of the hydrochar is lower and the explosive is stronger than coal used in blast furnace injection [2,18–20].

Based on the aforementioned reports, both biomass pyrolytic char and hydrochar have certain limitations. Utilizing either alone can lead to challenges such as elevated alkali metal content and safety risks in the blast furnace. Consequently, large-scale implementation of biomass in blast furnaces becomes challenging. Therefore, it becomes imperative to identify a process capable of simultaneously reducing alkali content and volatile matter in biomass, thereby achieving a composition closer to anthracite. However, existing research focuses solely on separate HTC or pyrolysis approaches for biomass treatment, with no information on combining these two processes. In this study, we propose a novel approach that integrates HTC and pyrolysis to treat biomass. Our aim is to comprehensively investigate microcrystalline parameters, chemical structure, functional group properties, and gasification characteristics to maximize energy density and minimize alkali content. Furthermore, there is a lack of research discussing the application pathway of biomass in blast furnaces, as well as the potential environmental and economic benefits associated with it.

In this study, maize straw (MS) was selected as the raw material. The primary hydrochar (HC) and pyrolytic char (PC) were obtained through initial treatment using hydrothermal carbonization (HTC) and pyrolysis, respectively. Subsequently, a secondary cross-upgrading treatment was applied to the primary samples to obtain pyrolysis products of HC (P-HC) and HTC products of PC (H-PC). Comprehensive investigations were conducted on the composition, transformation process, physicochemical structure, safety performance, and gasification properties of the resulting biochar. Furthermore, a comparison was made between the cross-upgraded biochar and Shenhua bituminous coal (SH) and Yangquan anthracite (YQ), which were two commonly used injection fuels in Chinese blast furnaces. The differences between cross-upgraded biochar and coal were analyzed. Finally, a biomass injection pathway for blast furnaces was proposed, and the environmental and economic benefits resulting from this injection were calculated. The study aims to identify suitable methods for high-quality biochar preparation and provide theoretical guidance for the application of biomass energy in steel production, power generation, and other relevant areas.

2. Experimental

2.1. Preparation of materials

Yangquan anthracite (YQ) was from Yangquan, Shanxi province of China. The Shenhua bituminous coal (SH) was from Shenmu, Shanxi province of China. MS used in this study was obtained from a farmland in Yuzhou, Henan province of China. To facilitate subsequent drying and loading operations, MS was crushed to less than 74 μm before the experiment. The above three samples were dewatered after drying oven at 105°C for 12 h.

2.2. Preparation of biochar

According to previous research [13,15], the optimal HTC parameters of MS are 280°C and heat preservation for 1 h, and the optimal pyrolysis parameters of MS are 600°C and heat preservation for 1 h. Therefore, the above experimental parameters were selected for the preparation of primary biochar. For the preparation of primary hydrochar, 20 g MS and 60 mL deionized water were added into a high-pressure reactor. After heating to 280°C at 10°C/min and holding for 1 h in an inert atmosphere, primary hydrochar (HC) was obtained. For the preparation of primary pyrolytic char (PC), 80 g MS was heated to 600°C at 20°C/min and carbonized for 1 h under nitrogen atmosphere. For the second treatment stage, PC was carried out to prepare the hydrochar of PC (H-PC), and HC was pyrolyzed to produce pyrolytic char of HC (P-HC). Therefore, HC and PC were defined as primary biochar, H-PC and P-HC as secondary biochar. Fig. 1 shows the schematic diagram of biomass cross-upgrading process.

2.3. Physicochemical properties

The chemical compositions of the samples (C/H/N/S) were measured by the elemental analyzer (Vario EL Cube), and the oxygen content was calculated by the difference. The proximate analysis of coals was measured according to GB/T212—2008, while those of biomass and biochar were measured according to GB/T 28732—2012, and the results of proximate analysis and ultimate analysis are shown in Table 1. The contents of alkali (K, Na) and Zn in the samples were determined by plasma spectrometer (Agilent 5900 ICP-OES). The high heating value (Q), mass yield ($\eta_{\text{Mass yield}}$), and energy yield ($\eta_{\text{Energy yield}}$) of the samples can be calculated by Eqs. (1)–(3) [15]:

$$Q = 0.3419w_C + 1.1783w_H + 0.1005w_S - 0.1034w_O - 0.0151w_N - 0.0211w_A \quad (1)$$

$$\eta_{\text{Mass yield}} = \frac{m_{\text{Biochar}}}{m_{\text{Feedstock}}} \times 100\% \quad (2)$$

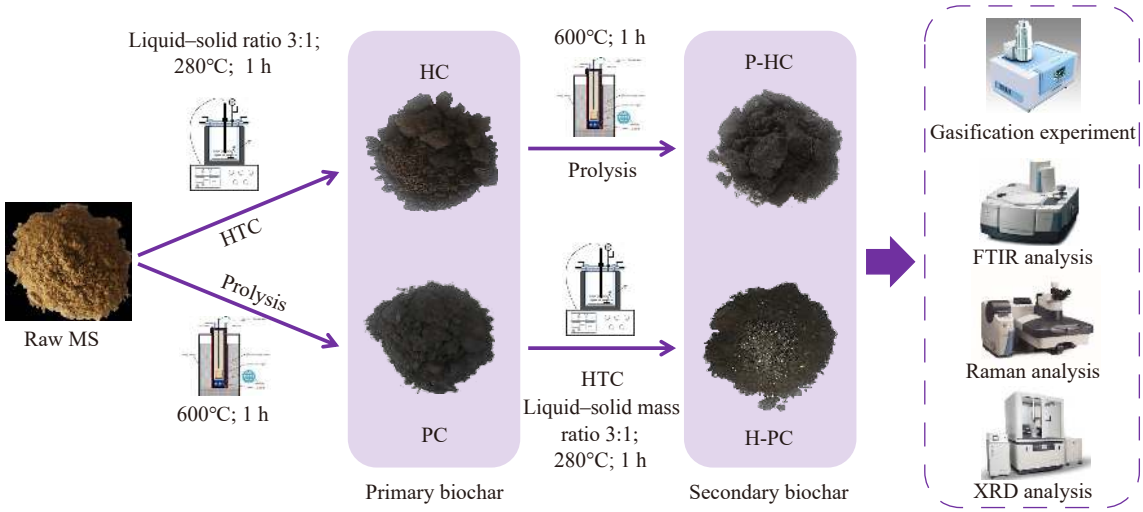

Fig. 1. Schematic diagram of biomass secondary cross-upgrading.

Table 1. Component analysis and high heating value of the sample

Sample	Proximate analysis / wt%			Ultimate analysis / wt%					Atomic ratio		Q / (MJ·kg^{-1})
	FC_d[a]	A_d	V_d	C	H	O[a]	N	S	O/C	H/C	
MS	19.31	6.00	74.69	46.27	5.837	41.35	0.54	0.00	0.670	1.514	18.62
HC	52.32	2.33	45.35	71.02	5.213	20.32	0.95	0.17	0.215	0.881	28.79
PC	68.83	15.49	15.68	74.27	2.923	6.44	0.77	0.10	0.065	0.472	28.38
H-PC	75.59	7.66	16.75	81.70	3.317	6.47	0.83	0.03	0.059	0.487	31.59
P-HC	80.60	3.21	16.19	85.27	3.208	6.94	1.36	0.02	0.061	0.451	32.74
YQ	80.55	11.40	8.05	82.92	2.500	1.47	1.09	0.62	0.013	0.362	31.55
SH	60.43	8.11	31.46	72.50	4.351	13.90	0.89	0.25	0.144	0.720	28.84

Note: [d] Dry basis; [a] Calculated by difference. FC—Fixed carbon; A—Ash; V—Volatile matter.

$$\eta_{\text{Energy yield}} = \eta_{\text{Mass yield}} \times \frac{Q_{\text{Biochar}}}{Q_{\text{Feedstock}}} \tag{3}$$

where w_C, w_H, w_S, w_O, and w_N represent the mass fraction of carbon, hydrogen, sulfur, oxygen, and nitrogen in the samples respectively, and w_A represents ash content; m_{Biochar} and $m_{\text{Feedstock}}$ represent mass of biochar and feedstock; Q_{Biochar} and $Q_{\text{Feedstock}}$ represent high heating value of biochar and feedstock, respectively.

Scanning electron microscopy (SEM, ZEISS EVO-18) with 20 kV acceleration voltage and 10 mm working distance was used to observe the apparent morphology of the sample at 1000 times magnification. Pore structure parameters were determined by automatic independent multi-station specific surface and sediment analyzer (Qudrasorb SI), BET method was used to obtain specific surface area (S_t). Fourier transform infrared spectrometer (FTIR spectrometer, iS50) was used to observe the changes and the difference in functional groups between biochar and coal. The order degree of carbon atoms in the samples was determined by Raman spectrometer (Lab RAMHR Evolution).

2.4. Gasification experiment

The gasification and combustion reaction occur at the same time in the raceway of BF. If the pulverized coal cannot be consumed in time, it will affect the operation of BF [21]. Biochar is a carbon-based fuel with combustion performance similar to coal, and the study of its gasification performance is of great significance to the industrial application.

The gasification experiment was carried out on a thermogravimetric balance (HCT-3, Henven Scientific Instrument Factory, China). During the experiment, 5 mg of the samples with particle size less than 74 μm were placed in a 3 mm × 1.5 mm corundum crucible and heated from 25 to 1200°C at a heating rate of 20°C/min, and then held for 5 min. The experiment was carried out in an atmosphere with CO_2 flow rate of 100 mL/min. The original experimental data obtained by the thermogravimetric balance can be substituted into Eqs. (4)–(5) to obtain the gasification conversion ratio (x) and gasification conversion rate (dx/dt) of each sample at the corresponding temperature. The comprehensive gasification characteristic index (S) was used to quantitatively compare the comprehensive gasification performance of all samples, and the calculation formula is shown in Eq. (5) [22].

$$x = \frac{m_t - m_0}{m_\infty - m_0} \tag{4}$$

$$S = \frac{(dx/dt)_{\max} \times (dx/dt)_{\text{mean}}}{T_i^2 \times T_f} \tag{5}$$

where $(dx/dt)_{\max}$ is the maximum weight loss rate, %·min^{-1}; $(dx/dt)_{\text{mean}}$ is the average weight loss rate, %·min^{-1}; T_i is the initial gasification temperature of fuel, °C; T_f is the end gasification temperature of fuel, °C.

2.5. Safety performance testing

The values of ignition point and explosiveness of fuel are very important parameters for BF operators [23]. In this paper, the ignition point value of the sample was measured by solid oxidation method and explosiveness was obtained by observing the return flame length of the sample in the long tube explosive detector. These test instruments and methods are shown in Fig. 2.

2.6. Kinetic model

The relationship between weight loss and time is usually used to characterize the gasification characteristics of samples, and the kinetic process in this process is worthy of further study [23]. In this study, volume model was used to fit the gasification reaction process of the sample. The volume model assumed that the gasifying agent was evenly distributed on the surface and inside of the carbon particles, and chemical reactions could occur at all active sites. Because of its high fitting reliability, it is widely used in the study of various gasification characteristics. Under thermal equilibrium, the kinetics of sample gasification reaction can be expressed as follows [24–25]:

$$\frac{\mathrm{d}x}{\mathrm{d}t} = k(T)f(x) \tag{6}$$

where x is the conversion rate of gasification reaction, %; T is the temperature when the conversion rate is x, K; t is the corresponding time when the conversion rate is x, s.

$k(T)$ is usually considered to satisfy the Arrhenius formula:

$$k(T) = A\exp\left(-\frac{E}{RT}\right) \tag{7}$$

where A stands for pre-exponential factor, E represents the apparent activation energy, kJ/mol; R stands for gas constant, 8.314 J/(mol·K).

$f(x)$ can be expressed as

$$f(x) = (1-x)^n \tag{8}$$

where n stands for the order of the reaction.

The gasification reaction takes place at a constant heating rate β ($\beta = \mathrm{d}T/\mathrm{d}t$), and Eq. (6) can be further characterized as follows [25–27]:

$$\frac{\mathrm{d}x}{(1-n)^n} = \frac{A}{\beta}\exp\left(-\frac{E}{RT}\right)\mathrm{d}T \tag{9}$$

In general, the gasification process of biomass can be considered as a first-order reaction [22]. Therefore, the integration of the above formula can be further obtained as follows:

$$\ln\left[-\frac{\ln(1-x)}{T^2}\right] = -\frac{E}{RT} + \ln\frac{AR}{\beta E} \tag{10}$$

Using $1/T$ as the X-axis and $\ln[-\ln(1-x)/T^2]$ as the Y-axis, we can obtain the slope $-E/R$ and the intercept $\ln(AR/\beta E)$.

3. Results and discussion

3.1. Proximate, ultimate analysis and yield analysis

The macromorphologies of different samples are shown in Fig. 3. After primary or secondary treatment, some changes have taken place in the apparent morphology of biomass [14,22]. The color of hydrochar after primary HTC is lighter than that after primary pyrolysis, so it can be inferred that primary pyrolysis has a stronger carbonization effect on biomass, which is also consistent with the results in Table 1. The color of P-HC is darker than that of H-PC, again verifying that pyrolysis has better carbonization effect than HTC. SH and PQ showed obvious graininess, and SH was glossier than YQ, suggesting that the deeper the carbonization, the darker the color of the sample.

Fig. 3 illustrates the macromorphologies of different samples. Significant changes in the apparent morphology of biomass have been observed after primary or secondary treatment [14,22]. Comparing the color of HC and PC, it can

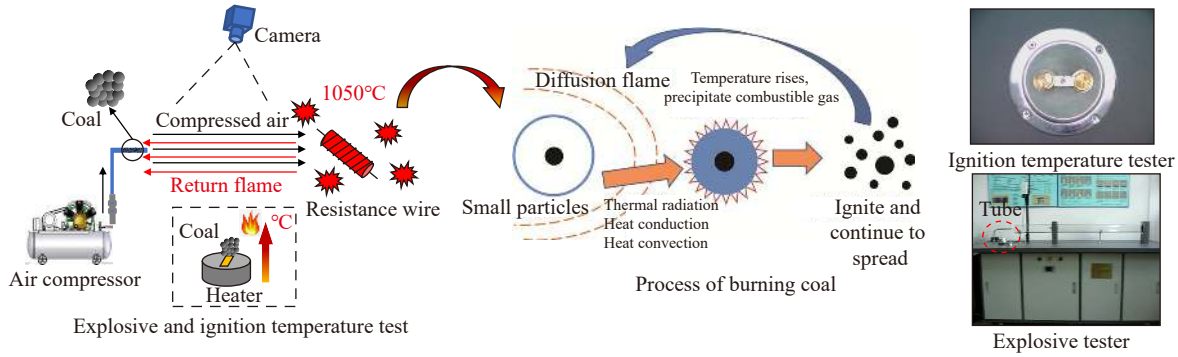

Fig. 2. Schematic diagram of ignition and explosive test.

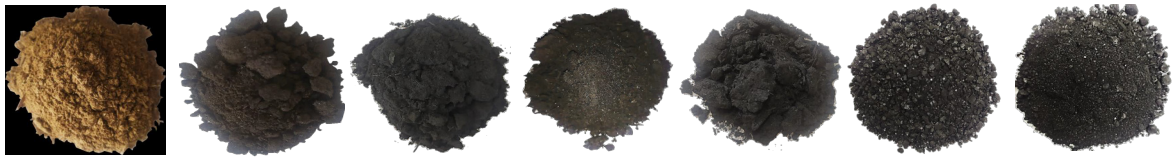

Fig. 3. Macromorphologies of different samples.

be inferred that PC has a stronger carbonization effect on biomass, which aligns with the findings presented in Table 1. Furthermore, the darker color of P-HC compared to H-PC further supports the notion that pyrolysis leads to better carbonization. Both SH and PQ exhibit a noticeable graininess, with SH being more glossy than YQ, indicating that the sample's color becomes darker with increased carbonization.

According to the results of Table 1, the FC of H-PC and P-HC is close to the level of YQ. The volatile components of HC and PC are 43.53wt% and 16.58wt%, respectively, and the volatile components of P-HC and H-PC are 16.19wt% and 16.75wt%, respectively. This indicates that pyrolysis can efficiently remove volatiles in the primary process. The ash content of H-PC and P-HC were 7.66wt% and 3.21wt% respectively, which indicates that HTC−prolysis can better remove ash from biomass and greatly increase the energy density of MS [28–32]. The high heating values of P-HC and H-PC are 32.74 and 31.59 MJ/kg, which are higher than YQ. The above results show that MS after secondary treatment can meet the demand of blast furnace injection.

Fig. 4(a) illustrates that the yields of biochar of the same grade are similar. The mass yield of primary biochar is approximately 38wt%, with an energy yield higher than 56%. After the cross-upgrading technology, the mass and energy yields of P-HC are higher than H-PC. Although the mass yield of P-HC and H-PC is around 1/4 of MS, the secondary biochar retains almost 70wt% of the mass and over 75% of the energy of the primary biochar. This suggests that the primary treatment stage has the most significant effect.

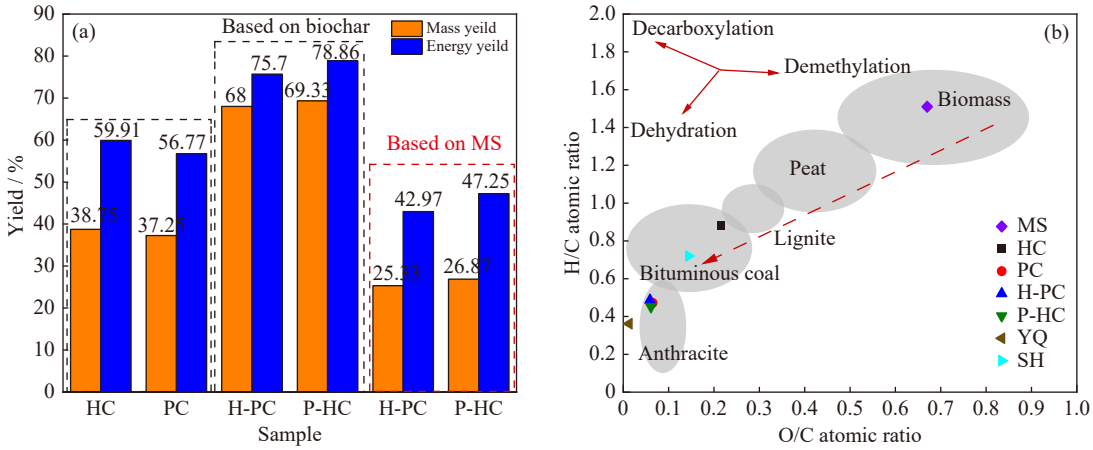

Fig. 4. (a) Yield and (b) Van Krevelen diagram of different samples.

To investigate the biomass upgrading process and the change in coal rank, the Van Krevelen diagram of the samples is presented in Fig. 4(b). HC is positioned in the bituminous coal region and is close to SH, which aligns with the findings of Wang *et al.* [15]. On the other hand, PC is in proximity to YQ, even though it is situated within the anthracite area. This demonstrates that pyrolysis exhibits a stronger capacity for dehydration and decarboxylation. Rodríguez Correa *et al.* [33] discovered that the thermal stability of pyrolytic char surpasses that of hydrochar. Consequently, the yield of activated carbon produced from pyrolytic char via heat treatment is higher compared to that of hydrochar. Similarly, due to the lower thermal stability of HC compared to PC, P-HC is positioned in the lower left area of HC after secondary upgrading, while PC and H-PC remain in essentially the same position. In general, all biochar is located within the anthracite region. Apart from HC, which has a high volatile content, the remaining biochar samples are positioned close to YQ. This signifies that secondary primary treatment can significantly enhance the quality of MS, making it a potential candidate for blast furnace injection fuel.

High content of alkali in the injection fuel can lead to cyclic accumulation and wall nodules in the BF shaft due to the low melting point and boiling points of alkali such as K, Na, and Zn, which are not conducive to the stable operation of the BF, which was considered as harmful elements for blast furnace [22]. Therefore, it is necessary to detect the contents of K, Na, and Zn in the samples, and the test results were shown in Table 2.

It can be seen from Table 2 that the content of K in MS and its biochar is much higher than the other two elements (Na, Zn). The harmful element contents of MS and PC are much higher than YQ and SH, which is consistent with the research results of many studies [14−16]. The content of harmful elements of PC is 3.3 times that of H-PC. Although the content of harmful elements in H-PC is about 3.3 times of YQ and 10 times of SH, it is undeniable that the total harmful element content of H-PC is lower than that of MS and PC. The content of harmful elements in HC is slightly increased after pyrolysis, but it is lower than that of YQ.

Table 2. Mass fraction of harmful elements wt%

Sample	K	Na	Zn	Total
MS	2.38	0.039	≤0.01	2.419–2.429
HC	0.34	0.031	≤0.01	0.371−0.381
PC	6.49	0.043	0.089	6.622
H-PC	1.91	0.041	0.10	2.051
P-HC	0.39	0.034	0.13	0.554
YQ	≤0.01	0.600	≤0.01	0.600−0.620
SH	≤0.01	0.180	≤0.01	0.180−0.200

It is worth noting that the K and Na metal contents of MS were substantially decreased after HTC treatment, which was attributed to the fact that as the HTC reaction proceeded, the components of the biomass samples were gradually decomposed into small-molecule organic acids dominated by carboxylic acids, leading to a decrease in the pH value of the HTC reaction environment, which facilitated the further removal of alkali metals and elemental Zn along with the discharging of the reaction waste stream. This is consistent with the authors' previous study, which also showed a consistent pattern [34]. However, after the pyrolysis treatment, K, Na, and Zn were enriched, which was due to the reaction environment in an inert atmosphere. The biomass itself could not be effectively removed from the ash, and with the increase in temperature its volatilization was removed and condensed to form tars, which were adhered to the stomata on the surface of the biomass, further preventing the removal of ash. Therefore, as the biomass yield decreases and the ash is enriched, the K, Na, and Zn assigned to the ash are similarly enriched, presenting an elevated mass fraction. Li *et al.* [35] similarly found that in pyrolytic pretreatment of samples such as corn cobs at elevated temperatures, the ash content of the samples likewise continued to increase as the temperature increased. For the cross-upgraded biochar, the alkali metal content of P-HC was only slightly enhanced as it was not affected by tar and ash enrichment. H-PC still contains a large number of hazardous elements because the PC has formed a tar and ash enrichment that cannot be completely removed by HTC.

Combined with the results in Table 1, it can be revealed that P-HC is a kind of biomass fuel with high calorific value, low sulfur and harmful element content. In addition, the application of H-PC to industrial furnaces will increase the alkali load of BF, but P-HC will not.

3.2. Microstructure analysis

SEM is a significant technique used to observe the microscopic surface structure of samples [22]. Fig. 5 presents the SEM images of the samples. The surface of MS appears relatively smooth with a few holes. On the other hand, HC exhibits numerous tiny holes and possesses an evident fibrous structure. In comparison to HC, PC displays a relatively loose structure. This suggests that under the experimental conditions, pyrolysis has a more detrimental impact on the structure of MS than HTC. The surface of P-HC shows a large number of holes, indicating the further removal of HC volatilization during pyrolysis. In contrast, H-PC features a smooth surface and a compact structure, similar to that of SH and YQ.

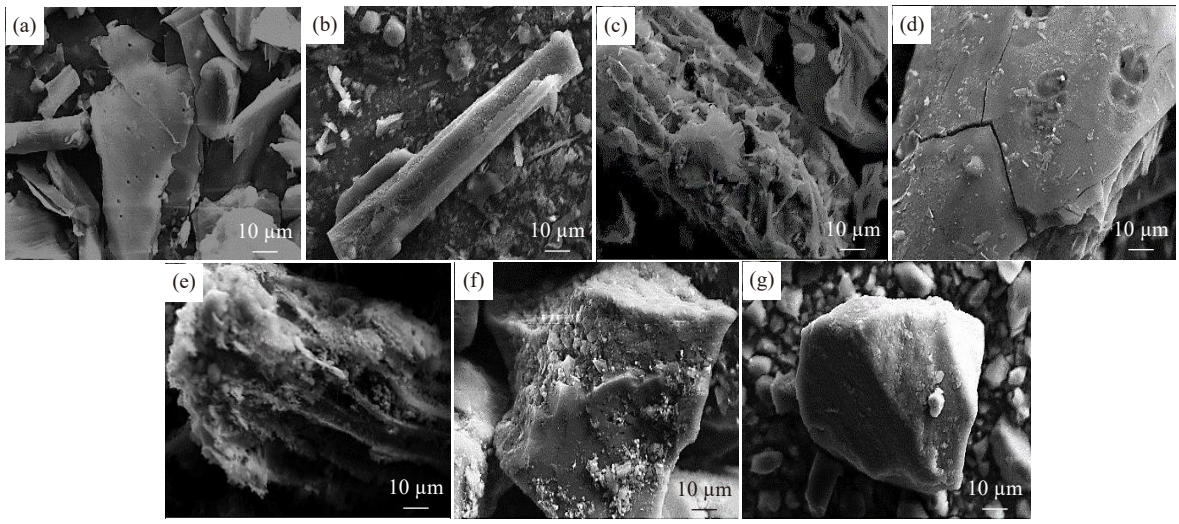

Fig. 5. SEM images of the samples: (a) MS; (b) HC; (c) PC; (d) H-PC; (e) P-HC; (f) SH; (g) YQ.

In order to quantitatively study the microstructure characteristics of the samples, the N_2 adsorption method was used to detect the total surface area (S_t), total pore volume (V_t), and average pore diameter (D_a) of the samples, as shown in Table 3. MS has smaller S_t than biochar [14,22]. In addition, the S_t value of biochar is larger than those of SH and YQ [2]. The S_t values of PC and P-HC are much larger than those of HC and H-PC, which is related to the strong devolatilization of pyrolysis. Wang *et al.* [15] found that when the HTC temperature was higher than 250°C, due to the significant increase in the pressure and permeability of water, the destructive ability of water to biochar increased, which softened the structure of the biochar and collapsed the pores, resulting in the S_t of biochar decreasing. Similar to previous study, after PC was upgrading by HTC at 280°C, the S_t and D_a of H-PC, the HTC product of PC, were significantly reduced. In addition, with the increase of the pyrolysis temperature of HC, the volatiles of HC were rapidly released to form many new and small pores, and the closed pores were opened, resulting in a

Table 3. Pore structure parameters

Sample	S_t / ($m^2 \cdot g^{-1}$)	V_t / ($cm^3 \cdot g^{-1}$)	D_a / nm
MS	0.93	3.01×10^{-3}	12.97
HC	6.08	2.22×10^{-3}	14.59
PC	51.75	3.49×10^{-3}	7.96
H-PC	8.29	1.40×10^{-3}	6.77
P-HC	74.48	4.98×10^{-3}	2.68
YQ	1.67	4.43×10^{-3}	12.38
SH	4.42	1.08×10^{-3}	9.77

significant increase in the S_t and V_t of biochar [14], so the S_t and V_t of P-HC were much higher than those of HC. The above results are also consistent with the SEM observations.

3.3. Physical and chemical structure analysis

The molecular arrangement and functional groups in biomass will change after secondary cross-upgrading [13,15]. As is shown in Fig. 6(a), the absorption characteristic peaks of the samples include –CH bending vibration peak (790 cm^{-1}), C–O absorption peak (1060 cm^{-1}), C=C tensile vibration peak (1605 cm^{-1}), C=O absorption peak (1735 cm^{-1}), CH_n absorption peak (2840–3000cm^{-1}), and –OH absorption peak (3200–3500 cm^{-1}). A large number of absorption peaks appear in the wavelength range of 1800–1000 cm^{-1}, indicating that MS has a large number of oxygen-containing functional groups [14]. The number of absorption peaks of functional groups decreases and the spectra of HC and PC becomes smoother compared to MS, indicating that both HTC and pyrolysis can remove functional groups from MS [15]. The spectrum of HC is similar to that of MS, indicating that HC still retains a large number of functional groups in MS, and this is the reason why HC has high volatile. In the spectra of PC, P-HC, and H-PC, the absorption peaks of C=C are obvious and the spectral curves are similar to SH and YQ, indicating that these three kinds of biochar contain a large number of functional groups similar to SH and YQ. In addition, the spectrum of P-HC in the range of 800–500 cm^{-1} showed some absorption peaks related to C=C and C–H and the side rings of alkanes. These results showed that the molecular structure of HC is destroyed during pyrolysis and the number of small molecules in P-HC increases, while H-PC does not have this phenomenon. This explains the smooth surface of H-PC and the large number of pores on the surface of P-HC in Fig. 5.

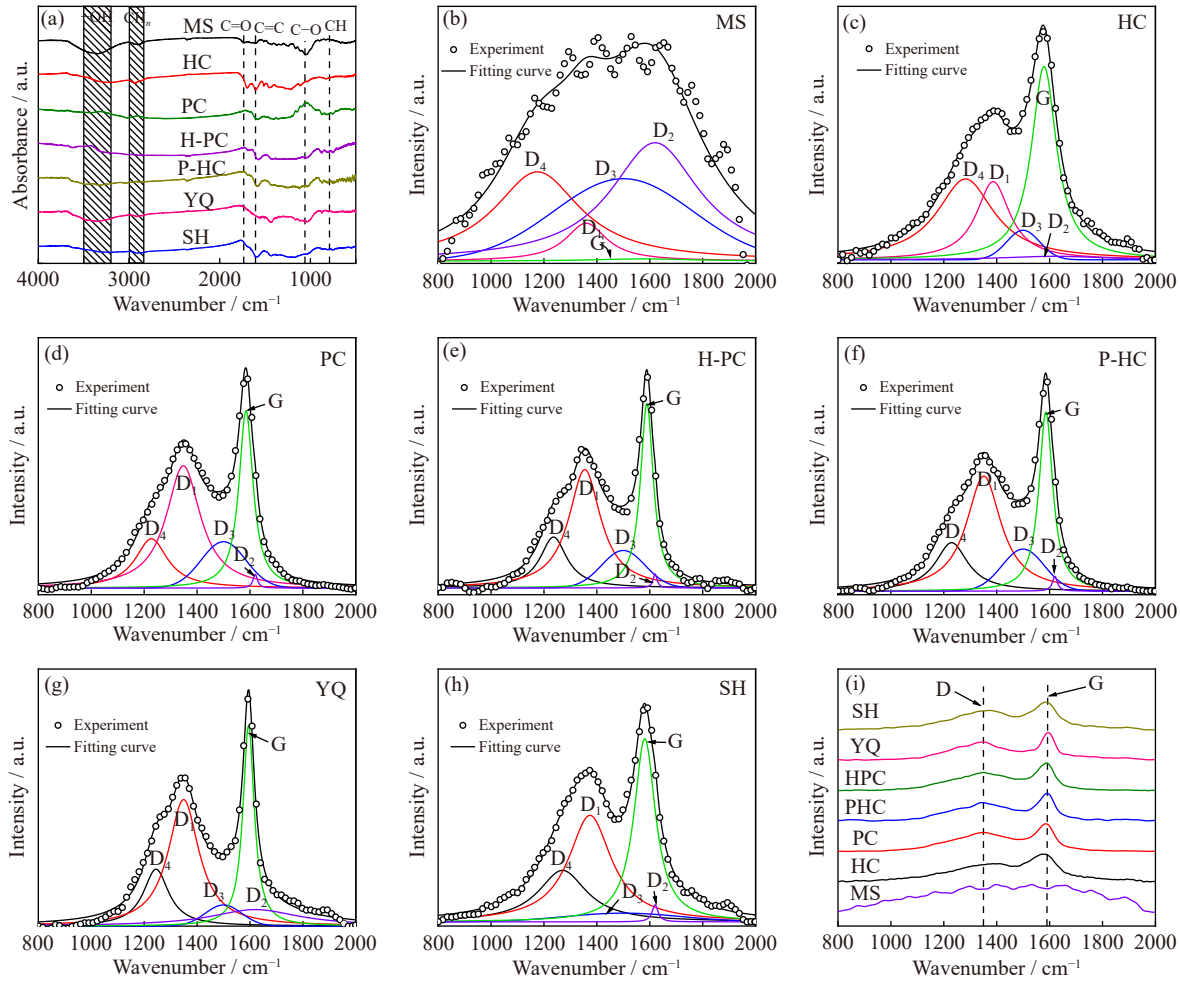

Fig. 6. (a) FTIR spectra of different samples. (b–h) Raman spectra of different samples: (b) MS; (c) HC; (d) PC; (e) H-PC; (f) P-HC; (g) YQ; (h) SH. (i) Peak-fitting diagram of different samples.

However, FTIR analysis alone cannot determine the degree of carbonaceous structure ordering. To address this limitation, Raman analysis was conducted on samples treated under different conditions, as depicted in Fig. 6(b)–(i). The Raman spectra of the various samples exhibit two prominent peaks at shifts of 1350 and 1600 cm^{-1}, corresponding to the D peak (amorphous carbon peak) and the G peak (graphite peak) [34–36]. In this study, the Lorentzian function was employed to fit the D_1, D_2, D_4, and G peaks, while the Gaussian function was utilized to fit the D_3 peak [37–38]. The characteristic parameters of the samples are displayed in Table 4.

The G peak of MS, which represents the stretching vibra-

Table 4. Raman peak-fitting characteristic values of the samples

Sample	I_{D1}	I_{D2}	I_{D3}	I_{D4}	I_G	I_{D3+D4}/I_G
MS	163.44	511.02	355.64	385.27	9.46	78.33
HC	215.91	9.59	81.41	223.13	534.21	0.57
PC	183.11	20.65	69.40	73.78	265.39	0.54
H-PC	51.99	6.19	16.45	22.35	81.06	0.48
P-HC	317.48	40.83	116.00	133.72	494.78	0.50
YQ	541.59	70.68	90.54	243.69	861.74	0.39
SH	210.94	23.45	28.99	188.83	459.96	0.47

Note: I_{D1}, I_{D2}, I_{D3}, I_{D4}, and I_G represent the peak intensities of D_1, D_2, D_3, D_4, and G, respectively. I_{D3+D4}/I_G represents the ratio of the sum of the peak intensities of D_3 and D_4 to the peak intensity of G.

tion of carbon atoms on the graphite sheet, is the weakest. This indicates that the arrangement of carbon atoms in MS is disordered [39]. The G peaks of PC and HC are stronger than that of MS and are also higher compared to the other sub-peaks. This suggests that both pyrolysis and HTC contribute to an improvement in the degree of carbon sequence in MS [14]. Among the Raman sub-peaks of HC, the D4 peak, representing the vibration of the olefin structure, is stronger than the D_1 peak, which represents structural defects and impurity atomic vibrations. However, in the Raman sub-peaks of PC, D_1 is stronger than D_4 [39]. This indicates that HC contains a significant amount of olefin structure, while PC contains a substantial amount of impurity atoms, which aligns with the results obtained from proximate analysis and FTIR.

Previous studies have shown that the value of I_{D3+D4}/I_G can better express the structural order degree [15,40]. The I_{D3+D4}/I_G values of PC and HC are higher than that of MS, indicating that HTC and pyrolysis could improve the order of carbon atoms in biomass [2,14], which is the same as observed in the peak-fitting diagram of the sample. As the devolatilization effect of pyrolysis is stronger than that of HTC, the number of disordered carbon atoms on the carbon lamellar of PC is less than that of HC, so the I_{D3+D4}/I_G of HC is larger than that of PC [33]. Because HC contains large number of disordered carbon atoms, some of the disordered carbon atoms are released from the HC in the form of volatile matter in the process of pyrolysis, making the I_{D3+D4}/I_G of P-HC lower than that of HC. However, the chemical bonds of some carbon atoms in the aromatic nucleus of HC are broken and combined with hydrogen atoms, or side rings of alkanes are formed during pyrolysis, so the carbon atom sequence degree in the carbon lamellar layer of P-HC is lower than that of H-PC [39]. The carbon atomic sequence degree on the graphite sheet of H-PC is the highest among all biochar, basically equal to that of SH, but much lower than that of YQ. The secondary processing treatment increased the size of carbonaceous crystallites and the graphitization degree of the biomass, leading to a more compact, orderly, and stable carbonaceous structure in the biochar.

Previous studies have demonstrated that the I_{D3+D4}/I_G value is a better indicator of the degree of structural order [15,40]. The I_{D3+D4}/I_G values of PC and HC are higher than that of MS, indicating that both HTC and pyrolysis enhance the order of carbon atoms in biomass, which is consistent with the observation in the sample peak fitting plots [2,14]. As pyrolysis exhibits a stronger devolatilization effect than HTC, the number of disordered carbon atoms on the carbon lamellae of PC is lower than that of HC, resulting in a higher I_{D3+D4}/I_G value for HC compared to PC [33]. Since HC contains a large number of disordered carbon atoms, some of which are released as volatiles during pyrolysis, the I_{D3+D4}/I_G value of P-HC is reduced. However, during pyrolysis, chemical bonds of certain carbon atoms in the aromatic nucleus of HC are broken, leading to their combination with hydrogen atoms or the formation of side rings of alkanes. Consequently, the carbon atom sequence degree in the carbon lamellar layer of P-HC is lower than that of H-PC [39]. The carbon atom sequence degree on the graphite sheet of H-PC is the highest among all biochar samples, approximately equal to that of SH but significantly lower than that of YQ. The secondary processing treatment results in larger carbonaceous crystallites and an increased degree of graphitization in the biomass, ultimately leading to a more compact, orderly, and stable carbonaceous structure in the biochar.

3.4. Gasification performance analysis

Fig. 7(a)–(b) shows that the gasification process of MS, HC, and SH can be divided into two obvious stages of devolatilization and fixed carbon gasification. In addition, other samples also showed slight weight loss before gasification indicating that all samples had two processes, which is the devolatilization and residual char gasification successively during the whole reaction process [41–42]. When pulverized coal is injected into the tuyere of BF, volatiles in coal are first precipitated [43]. If the pulverized coal fails to burn in time and a large number of the residual char fails to gasify in time, the permeability of BF will be affected [44–45]. Similarly, biochar is not guaranteed to be completely burnt in the raceway of BF when a large amount of biochar is injected [2]. Therefore, it is of great significance to study the gasification performance of biochar after devolatilization for the injection of biochar in BF [22].

The gasification conversion and conversion rate curves of residual char are shown Fig. 7(c)–(d), and the related characteristic parameters of gasification were obtained (Table 5). Although YQ has a larger *S* value, the gasification reaction of YQ has the highest temperature in the all samples. The D_G of HC is low, but the pyrolysis of HC during the heating process makes the gasification performance of the residual char of HC similar to P-HC, so their *R* values are very close. Al-

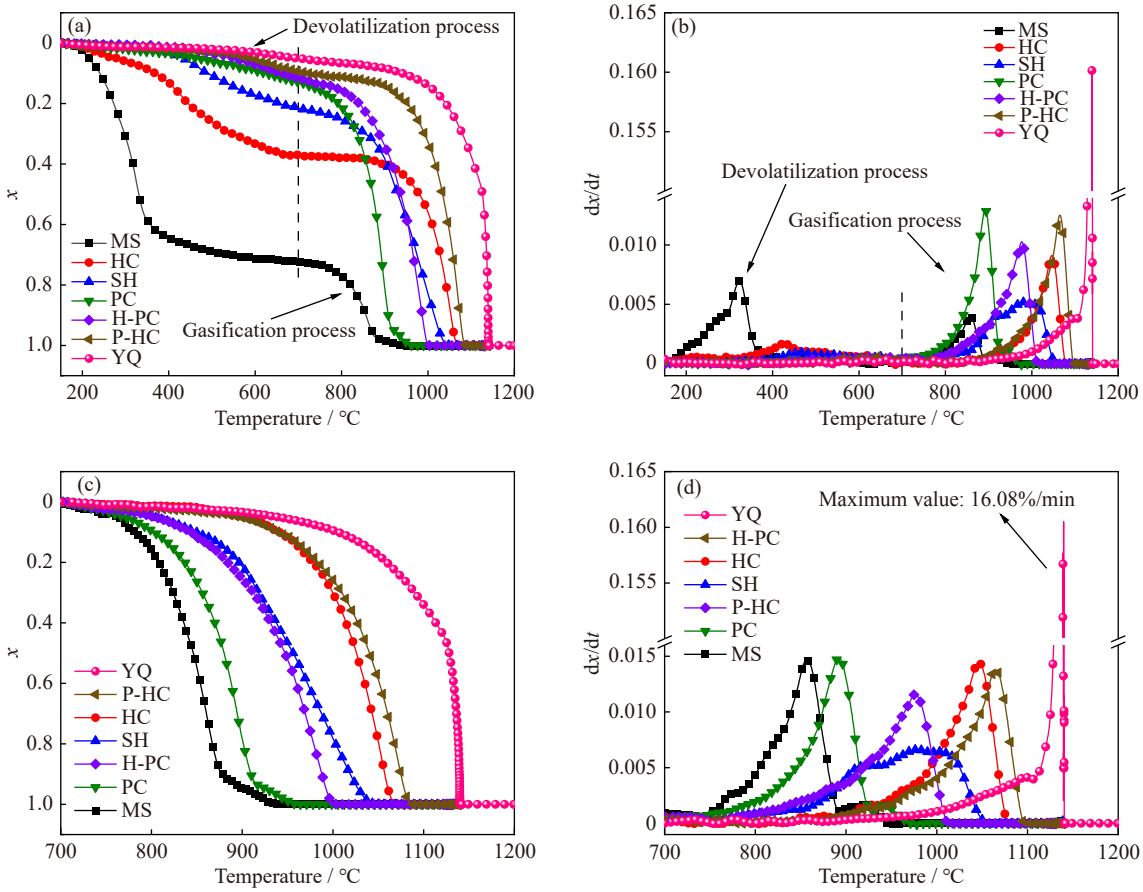

Fig. 7. Gasification curves (a) and gasification rate curves (b) of the samples; gasification curves (c) and gasification rate curves (d) of residual char.

Table 5. Gasification characteristics of carbon residue

Sample	T_i / °C	T_f / °C	$(dx/dt)_{mean}$ / (%·min^{-1})	$(dx/dt)_{max}$ / (%·min^{-1})	S / 10^{-9}
MS	762	900	0.65	1.47	1.83
HC	907	1060	0.58	1.45	0.96
PC	771	926	0.58	1.49	1.57
H-PC	803	993	0.47	1.16	0.85
P-HC	897	1080	0.49	1.38	0.78
YQ	939	1140	3.63	16.08	58.07
SH	803	1028	0.28	0.66	0.28

though P-HC has a large S_t, the catalytic effect of alkali on the gasification reaction of HC and P-HC is not significant due to the low content, so the temperature required for the gasification reaction of HC and P-HC is higher than that of H-PC [46]. The D_G of H-PC is lower than that of SH, but the content of alkali and the value of S_t is higher, so the gasification temperature of H-PC is lower [47]. There is an obvious turning point in the gasification curves of PC and MS at 860 and 895°C, which is related to the volatilization of alkali within this temperature range [48]. The above results show that the gasification reaction of secondary biochar is easier than that of YQ. Therefore, the gasification performance of the secondary biochar meets the BF requirements.

3.5. Safety performance analysis

As can be seen in Table 6, the mean ignition temperature (T_{mean}) and mean tempering length (L_{mean}) of the samples were used as evaluation parameters for the ignition point and explosiveness of the samples, where T_1 and T_2 represent ignition temperatures of different experiments, and L_1 and L_2 represent the tempering lengths of different experiments. When the L_{mean} value of the sample is greater than 400 mm, the sample is considered to have strong explosiveness, and if it is greater than or equal to 800 mm, it indicates that the sample has very strong explosiveness [26].

The ignition points of YQ and SH are 410.5 and 346.5°C, respectively. Since the volatile content of MS and HC is higher than that of SH, the ignition temperature of MS and HC is lower than that of SH. SH and HC are very strong explosive due to the fact that the L_{mean} is more than 800 mm. The L_{mean} of MS is 559.5 mm, indicating that MS has strong explosiveness. For PC, H-PC, and P-HC, they have slightly

Table 6. Ignition point and explosive results of the samples

Sample	Ignition temperature / °C			Return flame length / mm		
	T_1	T_2	T_{mean}	L_1	L_2	L_{mean}
MS	269.4	265.2	267.3	563	556	559.5
HC	332.1	328.8	330.5	≥800	≥800	≥800
PC	412.6	409.1	410.9	0	0	0
P-HC	432.0	415.3	423.7	0	0	0
H-PC	420.2	421.5	420.9	0	0	0
YQ	421.3	399.7	410.5	0	0	0
SH	347.2	345.8	346.5	≥800	≥800	≥800

higher ignition points than YQ, but are not explosive. The above results show that the safety performance of secondary biochar is similar to or even better than that of anthracite. Therefore, the biochar prepared by the new technology can meet the safety requirements of injection fuel.

3.6. Kinetic analysis

Biochar is a porous medium, and the chemical reaction mainly occurs on the inner surface of the hole: after the gas diffuses from the outside to the surface of the particle, it must overcome the resistance of pore diffusion to reach the inner surface of the hole to react. It includes adsorption, surface reaction, and desorption processes, which all involve the change of chemical bond and belong to the category of chemical processes. In order to quantitatively characterize the gasification reaction characteristics of samples, it is necessary to adopt a kinetic model to clarify the reaction mechanism of the gasification process. In this study, the volume model was used to fit the gasification reaction process of the sample, and the results are shown in Fig. 8(a). It can be seen that the volume model has a high degree of fitting to the experimental data, and the value of fitting degree R^2 is basically above 0.95, which indicates the correctness of the selection of the volume model.

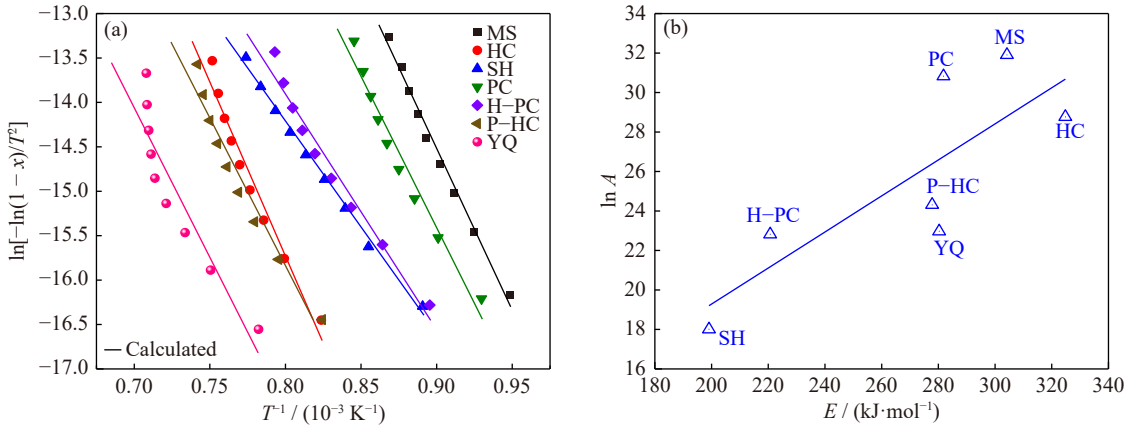

Fig. 8. (a) Kinetic model fitting results; (b) ln *A* versus *E* of different samples.

According to the results in Table 7, the apparent activation energy (E) of the sample gasification reaction ranges from 199.1 to 324.8 kJ/mol. Among them, the HC and SH have the highest and lowest E, respectively, which is not consistent with the test results. It is generally believed that the lower the E in the reaction process, the lower the energy barrier required for the reaction of the sample. However, in this study, the MS has the best gasification performance, but its E was very high. The YQ with the worst gasification reaction did not have the highest E. In addition, it is also observed from Fig. 8(b) that the pre-exponential factor (A) and E of the sample showed an obvious positive linear relationship, which Agrawal [46] calls "compensation effect." The gasification reaction speed of the sample is affected by both E and A. The smaller the value of E, the more molecules will be easily activated; the larger the value, the more molecules will collide and promote the gasification reaction. This may be a mathematical statistical deviation, but it is more caused by the uneven carbon structure of the sample. It should be noted that the current discussion is about the kinetic analysis of residual carbon in gasification reaction. MS has been reacted about 70% before 700°C, and MS at this time is equivalent to highly dense carbon materials with a large number of volatiles removed. In general, on small molecule systems with low condensation, the activation energy to overcome for gasification reactions is relatively small, so the activation will have an effect on a small number of carbon atoms, resulting in relatively few active chemical reaction sites [47–48]. However, it is worth noting that molecular clusters with higher condensation degrees exhibit higher activation energies. This is because the activation of sites on a specific aromatic ring cluster triggers a chain reaction involving numerous carbon atoms on the condensed aromatic ring cluster, resulting in a significant value of A. Consequently, this phenomenon can

Table 7. Kinetic parameters of the sample

Sample	T / °C	E / (kJ·mol^{-1})	Slope / 10^4	R^2	A	lnA/E
MS	781.5–878.2	304.2	–3.659	0.9895	7.19×10^{13}	0.105
HC	940.9–1057.5	324.8	–3.907	0.9652	3.12×10^{12}	0.089
PC	802.6–909.9	281.8	–3.390	0.9675	2.44×10^{13}	0.109
P-HC	940.0–1075.0	277.8	–3.342	0.9567	3.62×10^{10}	0.088
H-PC	843.7–988.1	220.7	–2.655	0.9713	8.10×10^{9}	0.103
YQ	1005.4–1139.5	280.3	–3.372	0.8568	9.47×10^{9}	0.082
SH	849.7–1019.1	199.1	–2.395	0.9946	6.62×10^{7}	0.090

explain the relatively high activation energy observed in MS. Finally, similar to R for gasification characteristics, lnA/E is also introduced in this paper to measure the synergistic effect of A and E on gasification reaction characteristics. It is believed that the larger the value of lnA/E, the better the gasification reaction characteristics of the sample, and the smallest lnA/E of YQ, resulting in higher completion temperature and poor gasification reaction. lnA/E of MS is 0.105, and the effect of A on the gasification characteristics is greater than that of E, resulting in the best gasification reaction characteristics. The existence of "compensation effect" indicates that the gasification reaction of biochar is a complex process, which needs to be further studied in the future.

By comparing the chemical composition, physicochemical characteristics, and gasification characteristics of different samples, P-HC is considered to be the most suitable biochar product for blast furnace injection. P-HC has higher yield, higher energy density, and better gasification characteristics. After being injected into the blast furnace air outlet, it reacts preferentially with CO_2, thus protecting the coke from melting losses and reducing coke consumption and CO_2 emissions. After being injected into the blast furnace air nozzle, it reacts preferentially with CO_2, thus protecting the coke from dissolution losses and reducing coke consumption and CO_2 emissions.

Although an optimal biochar preparation route has been proposed, the commercialization of this process still requires further consideration. Therefore, it is crucial to focus on the early establishment of large-scale production lines for HTC. In terms of the future application of biochar in blast furnace injection, the development of a continuous reactor poses a significant challenge for the large-scale commercialization of HTC. Continuous reactors are more automated, more controllable, and less dependent on human resources than current batch reactors, thus allowing for longer run times. This eliminates time and cost waste associated with heating and cooling in each production cycle. However, ongoing research in this area is insufficient and significant efforts are needed, particularly in developing a specialized delivery system that enables the continuous supply of biomass and water to the HTC reactor.

4. Application path and environmental benefit analysis of blast furnace injection

According to the research results in section 3, P-HC has great potential to be used as fuel for blast furnace injection. Therefore, this study puts forward the process route of applying P-HC to blast furnace injection (Fig. 9), combining biochar production and blast furnace injection, in order to provide guidance for the future development of biomass injection in China's iron and steel industry. In this process, MS and water are first added to the storage bunker for HTC treatment. After evenly mixing and preheating, the biomass is transported to the HTC high-pressure reactor to prepare primary biochar. The HTC process generates a large amount of biomass tar dissolved in water. Therefore, after the completion of HTC, the waste liquid needs to be separated from the oil and water, and the water obtained is returned to the system for recycling [4,17,25]. The HC obtained will be further pyrolyzed to obtain P-HC. After weighing, P-HC is transported to the stock bunker and then together with the raw coal to the raw coal bunker. After being ground to 200 mesh, they are collected by cloth bags to the pulverized coal bunker, where they are fully mixed and evenly transported by high-pressure nitrogen, and evenly distributed to the blast furnace tuyere for combustion through the distributor. It is worth noting that the combustion of blast-furnace gas and combustion-supporting air in the combustor provides heat sources not only for the coal mill, but also for HTC and pyrolysis, and the hydrogen-rich gas collected through the HTC and pyrolysis process is transported to the combustor for use as fuel. In addition, the enthalpy heat of slag in blast furnace production process can also provide sufficient heat source for HTC and pyrolysis, so as to realize the interaction of the three processes.

Biomass, as a carbon-neutral and clean energy source, replaces some of the pulverized coal applied in blast furnace injection, which is an important way to alleviate the pressure of energy consumption in the ironmaking process. Eq. (11) was used to calculate the CO_2 reduction amount (ΔC) by injecting biochar in blast furnace:

$$\Delta C = r_{\text{Coal}} \times \gamma \times w_{\text{C(Coal)}} \times \frac{Q_{\text{Biochar}}}{Q_{\text{Coal}}} \times \frac{44}{12} \times \eta \tag{11}$$

where r_{Coal} represents coal ratio, and the coal ratio of China BF is usually 160 kg/t; γ represents the ratio of replacing injection coal. China's blast furnaces usually adopt a fuel structure of 60wt% anthracite/40wt% bituminous coal, so 40wt% was taken in this study; $w_{\text{C(Coal)}}$ represents the C content of injection coal, usually 75%; Q_{Biochar} represents the heating value of biochar; Q_{Coal} represents the heating value of injection coal, usually 30 MJ·kg^{-1}; 44 and 12 represent the molar

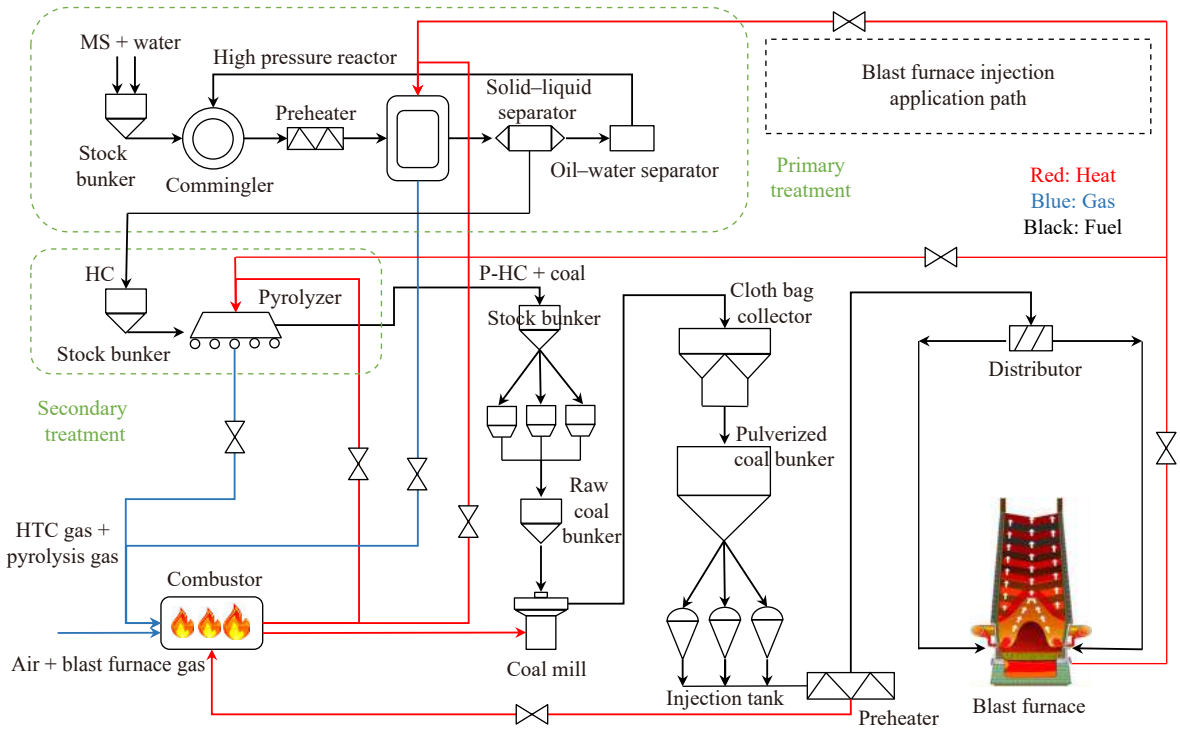

Fig. 9. Coupled cogeneration process route of biomass char preparation and blast furnace injection proposed in this paper.

mass of CO_2 and C, respectively; η represents BF gas utilization and the corresponding value for BF in China is usually 0.5.

The CO_2 emission reduction results were determined for HC, PC, H-PC, and P-HC with a biomass addition ratio of 40%. The calculated ΔC values for the four samples were 84.45, 83.24, 92.66, and 96.04 kg/t, respectively. These results indicate that utilizing biomass as a component of blast furnace injection fuel can achieve secondary utilization of waste biomass resources while simultaneously reducing carbon emissions from blast furnace injection. This approach offers significant environmental benefits.

5. Conclusions

(1) This paper conducted a systematic analysis of the composition, yield, physicochemical structure, and gasification performance of secondary biochar (H-PC and P-HC). The results demonstrate that the secondary cross-treatment process significantly enhances the applicability of biochar in blast furnace injection.

(2) The H/C and O/C atomic ratios of secondary biochars closely resemble those of YQ, and their degree of graphitization is similar to that of SH. This similarity in the characteristics of secondary biochar and SH results in similar gasification properties. However, the high heating value of secondary biochar surpasses that of SH, and even exceeds that of YQ. Consequently, P-HC is more suitable than H-PC for replacing coal in blast furnace injection.

(3) The volume model effectively fits the kinetics of the gasification reaction in the sample, with R^2 values exceeding 0.95. The activation energy (E) of the sample varies from 199.1 to 324.8 kJ/mol. Furthermore, the linear relationship between E and A confirms the presence of the kinetic compensation effect during the gasification process of the samples.

(4) A path for the application of P-HC to blast furnace injection and the possible environmental benefits are proposed and calculated. In this integrated process, HTC, pyrolysis, and blast furnace production can realize the circulation of matter and energy within the systems. P-HC has the greatest emission reduction potential, which can reduce 96.04 kg/t instead of 40% coal injection, and has great environmental benefits.

Acknowledgements

This work was financially supported by the National Key R&D Program of China (No. 2022YFE0208100), the National Natural Science Foundation of China (No. 5274316), the Key Research and Development Plan of Anhui Province, China (No. 202210700037), and the Major Science and Technology Project of Xinjiang Uygur Autonomous Region, China (No. 2022A01003).

Conflict of Interest

Jianliang Zhang is an editorial board member for this journal and was not involved in the editorial review or the decision to publish this article. The authors have no financial or proprietary interests in any material discussed in this article.

References

[1] J.L. Zhang, H.Y. Fu, Y.X. Liu, *et al.*, Review on biomass metallurgy: Pretreatment technology, metallurgical mechanism and

process design, *Int. J. Miner. Metall. Mater.*, 29(2022), No. 6, p. 1133.
[2] J. Zhao, H.B. Zuo, J.S. Wang, *et al*., The mechanism and products for co-thermal extraction of biomass and low-rank coal with NMP, *Int. J. Miner. Metall. Mater.*, 26(2019), No. 12, p. 1512.
[3] J.L. Zhang, J. Guo, G.W. Wang, *et al*., Kinetics of petroleum coke/biomass blends during co-gasification, *Int. J. Miner. Metall. Mater.*, 23(2016), No. 9, p. 1001.
[4] H.B. Zuo, W.W. Geng, J.L. Zhang, *et al*., Comparison of kinetic models for isothermal CO_2 gasification of coal char–biomass char blended char, *Int. J. Miner. Metall. Mater.*, 22(2015), No. 4, p. 363.
[5] N. Karali, T.F. Xu, and J. Sathaye, Reducing energy consumption and CO_2 emissions by energy efficiency measures and international trading: A bottom-up modeling for the U.S. iron and steel sector, *Appl. Energy*, 120(2014), p. 133.
[6] M, Hasanuzzaman, N.A. Rahim, M. Hosenuzzaman, *et al*., Energy savings in the combustion based process heating in industrial sector, *Renewable Sustainable Energy Rev.*, 16(2012), No. 7, p. 4527.
[7] K. Yan, C.W. Liu, L.P. Liu, *et al*., Pyrolysis behaviour and combustion kinetics of waste printed circuit boards, *Int. J. Miner. Metall. Mater.*, 29(2022), No. 9, p. 1722.
[8] S.N. Xiu and A. Shahbazi, Bio-oil production and upgrading research: A review, *Renew. Sustainable Energy Rev.*, 16(2012), No. 7, p. 4406.
[9] R. Saidur, E.A. Abdelaziz, A. Demirbas, M.S. Hossain, and S. Mekhilef, A review on biomass as a fuel for boilers, *Renewable Sustainable Energy Rev.*, 15(2011), No. 5, p. 2262.
[10] Q. Gao, G. Zhang, H. Zheng, *et al*., Combustion performance of pulverized coal and corresponding kinetics study after adding the additives of Fe_2O_3 and CaO, *Int. J. Miner. Metall. Mater.*, 30(2023), No. 2, p. 314.
[11] D. Zhang, H. Fan, B. Zhao, *et al*., Development of biomass power generation technology at home and abroad, *Huadian Technol.*, 43(2021), No. 03, p. 70.
[12] G. Wang, J. Zhang, J. Shao, *et al*., Thermal behavior and kinetic analysis of co-combustion of waste biomass/low rank coal blends, *Energy Convers. Manage.*, 124(2016), p. 414.
[13] P. Wang, G.W. Wang, J.L. Zhang, J.Y. Lee, Y.J. Li, and C. Wang, Co-combustion characteristics and kinetic study of anthracite coal and palm kernel shell char, *Appl. Therm. Eng.*, 143(2018), p. 736.
[14] Y.S. Sun, Y.X. Han, Y.F. Li, *et al*., Formation and characterization of metallic iron grains in coal-based reduction of oolitic iron ore, *Int. J. Miner. Metall. Mater.*, 24(2017), No. 2, p. 123.
[15] G.W. Wang, J.L. Zhang, J.Y. Lee, *et al*., Hydrothermal carbonization of maize straw for hydrochar production and its injection for blast furnace, *Appl. Energy*, 266(2020), art. No. 114818.
[16] J. Minaret and A. Dutta, Comparison of liquid and vapor hydrothermal carbonization of corn husk for the use as a solid fuel, *Bioresour. Technol.*, 200(2016), p. 804.
[17] H. Fatehi and X.S. Bai, Structural evolution of biomass char and its effect on the gasification rate, *Appl. Energy*, 185(2017), p. 998.
[18] Z.G. Liu, A. Quek, S. Kent Hoekman, *et al*., Production of solid biochar fuel from waste biomass by hydrothermal carbonization, *Fuel*, 103(2013), p. 943.
[19] T.L. Eberhardt, W.J. Catallo, and T.F. Shupe, Hydrothermal transformation of Chinese privet seed biomass to gas-phase and semi-volatile products, *Bioresour. Technol.*, 101(2010), No. 11, p. 4198.
[20] M. Goto, R. Obuchi, T. Hirose, *et al*., Hydrothermal conversion of municipal organic waste into resources, *Bioresour. Technol.*, 93(2004), No. 3, p. 279.
[21] M.I.G. Miranda, C.I.D. Bica, S.M.B. Nachtigall, *et al*., Kinetical thermal degradation study of maize straw and soybean hull celluloses by simultaneous DSC–TGA and MDSC techniques, *Thermochim. Acta*, 565(2013), p. 65.
[22] W. Liang, G.W. Wang, K.X. Jiao, *et al*., Conversion mechanism and gasification kinetics of biomass char during hydrothermal carbonization, *Renew. Energy*, 173(2021), p. 318.
[23] H. Guo, Y. Cheng, L. Wang, *et al*., Experimental study on the effect of moisture on low-rank coal adsorption characteristics, *J. Nat. Gas Sci. Eng.*, 24(2015), p. 245.
[24] J. Yu, A. Tahmasebi, Y. Han, *et al*., A review on water in low rank coals: The existence, interaction with coal structure and effects on coal utilization, *Fuel Process. Technol.*, 106(2013), p. 9.
[25] S. Dey, Enhancement in hydrophobicity of low rank coal by surfactants—A critical overview, *Fuel Process. Technol.*, 94(2012), No. 1, p. 151.
[26] H.B. Jiang, J.L. Zhang, J.X. Fu, *et al*., Properties and structural optimization of pulverized coal for blast furnace injection, *J. Iron Steel Res. Int.*, 18(2011), No. 3, p. 6.
[27] A. Murao, Y. Kashihara, K. Takahashi, *et al*., Effect of natural gas injection into blast furnace on combustion efficiency of pulverized coal, *Tetsu-to-Hagane*, 101(2015), No. 12, p. 653.
[28] Z.F. Peng, X.J. Ning, G.W. Wang, *et al*., Structural characteristics and flammability of low-order coal pyrolysis semi-coke, *J. Energy Inst.*, 93(2020), No. 4, p. 1341.
[29] H. Dang, G.W. Wang, C.M. Yu, *et al*., Study on chemical bond dissociation and the removal of oxygen-containing functional groups of low-rank coal during hydrothermal carbonization: DFT calculations, *ACS Omega*, 6(2021), No. 39, p. 25772.
[30] N. Zhang, G.W. Wang, C.M. Yu, *et al*., Physicochemical structure characteristics and combustion kinetics of low-rank coal by hydrothermal carbonization, *Energy*, 238(2022), art. No. 121682.
[31] S.W. Du, W.H. Chen, and J. Lucas, Performances of pulverized coal injection in blowpipe and tuyere at various operational conditions, *Energy Convers. Manage.*, 48(2007), No. 7, p. 2069.
[32] H.K. Li, Y.J. Wang, Jiao K., *et al.*, Study on alkali circulation process and its influence on coke ratio in blast furnace, [in] *10th International Symposium on High-Temperature Metallurgical Processing*, San Antonio, 2019
[33] C. Rodríguez Correa, M. Stollovsky, T. Hehr, *et al*., Influence of the carbonization process on activated carbon properties from lignin and lignin-rich biomasses, *ACS Sustainable Chem. Eng.*, 5(2017), No. 9, p. 8222.
[34] H. Dang, R.S. Xu, J.L. Zhang, *et al*., Hydrothermal carbonization of waste furniture for clean blast furnace fuel production: Physicochemical, gasification characteristics and conversion mechanism investigation, *Chem. Eng. J.*, 469(2023), art. No. 143980.
[35] R.P. Li, J.L. Zhang, G.W. Wang, *et al*., Study on CO_2 gasification reactivity of biomass char derived from high-temperature rapid pyrolysis, *Appl. Therm. Eng.*, 121(2017), p. 1022.
[36] O. Beyssac, B. Goffé, J.P. Petitet, *et al*., On the characterization of disordered and heterogeneous carbonaceous materials by Raman spectroscopy, *Spectrochim. Acta Part A: Mol. Biomol. Spectrosc.*, 59(2003), No. 10, p. 2267.
[37] Q. He, L. Ding, A. Raheem, *et al*., Kinetics comparison and insight into structure-performance correlation for leached biochar gasification, *Chem. Eng. J.*, 417(2021), art. No. 129331.
[38] N. Zhang, G.W. Wang, J.L. Zhang, *et al*., Study on co-combustion characteristics of hydrochar and anthracite coal, *J. Energy Inst.*, 93(2020), No. 3, p. 1125.
[39] A. Mosqueda, J.T. Wei, K. Medrano, *et al*., Co-gasification reactivity and synergy of banana residue hydrochar and anthracite coal blends, *Appl. Energy*, 250(2019), p. 92.
[40] R.V.P. Antero, A.C.F. Alves, S.B. de Oliveira, *et al*., Challenges and alternatives for the adequacy of hydrothermal car-

bonization of lignocellulosic biomass in cleaner production systems: A review, *J. Cleaner Prod.*, 252(2020), art. No. 119899.

[41] H.Y. Gong, Y.D. Huang, H.Y. Hu, *et al*., The potential oxidation characteristics of $CaCr_2O_4$ during coal combustion with solid waste in a fluidized bed boiler: A thermogravimetric analysis, *Chemosphere*, 263(2021), art. No. 127974.

[42] Q. Hu, H.P. Yang, H.S. Xu, *et al*., Thermal behavior and reaction kinetics analysis of pyrolysis and subsequent *in situ* gasification of torrefied biomass pellets, *Energy Convers. Manage.*, 161(2018), p. 205.

[43] S. Nomura and T.G. Callcott, Maximum rates of pulverized coal injection in ironmaking blast furnaces, *ISIJ Int.*, 51(2011), No. 7, p. 1033.

[44] C.L. Zhang, G.W. Wang, X.J. Ning, *et al*., Numerical simulation of combustion behaviors of hydrochar derived from low-rank coal in the raceway of blast furnace, *Fuel*, 278(2020), art. No. 118267.

[45] Y.H. Zhou, P. Zhou, J.Y. Dan, *et al*., Effects of single lance configuration on coal combustion process in tuyere from viewpoint of coal plume, *J. Iron Steel Res. Int.*, 28(2021), No. 7, p. 785.

[46] R.K. Agrawal, On the compensation effect, *J. Therm. Anal.*, 31(1986), No. 1, p. 73.

[47] P.J. Barrie, The mathematical origins of the kinetic compensation effect: 2. the effect of systematic errors, *Phys. Chem. Chem. Phys.*, 14(2012), No. 1, p. 327.

[48] K. Yip, E. Ng, C.Z. Li, *et al*., A mechanistic study on kinetic compensation effect during low-temperature oxidation of coal chars, *Proc. Combust. Inst.*, 33(2011), No. 2, p. 1755.